THE JOURNAL OF PHYSICAL CHEMISTRY C

Article

pubs.acs.org/JPCC

Hydrogen Storage in Palladium Hollow Nanoparticles

Felipe J. Valencia,[†,¶] Rafael I. González,[†,¶] Diego Tramontina,[‡,§] José Rogan,[†,¶] Juan Alejandro Valdivia,[†,¶] Miguel Kiwi,[*,†,¶] and Eduardo M. Bringa[‡]

[†]Departamento de Física, Facultad de Ciencias, Universidad de Chile, Casilla 653, Santiago, Chile 7800024

[‡]Facultad de Ciencias Exactas y Naturales, Universidad Nacional de Cuyo, Mendoza, 5500, Argentina, and CONICET, Argentina

[¶]Centro para el Desarrollo de la Nanociencia y la Nanotecnología, CEDENNA, Avda. Ecuador 3493, Santiago, Chile 9170124

[§]Instituto de Bioingeniería, Universidad de Mendoza, IBio-UM, Mendoza M5502BZG, Argentina

ABSTRACT: The potential and properties of palladium hollow nanoparticles (hNPs) as a possible H storage material are explored by means of classical molecular dynamics (MD) simulations. First, we study the stability of pure Pd hNPs for different sizes and thicknesses, obtaining good agreement with experimental results for nanometer size Pd hNP. Next we add, every 100 fs, single H atoms into the NP cavity. During the first stages of the simulation, our results show hydride formation on the inner surface, similar to what has been observed in experiments on Pd surfaces and NPs. Formation of the Pd hydride decreases the absorption rate, and H gas is formed inside the cavity. The maximum H gas pressure that is reached is of 7 GPa, before fractures appear in the hNP, and consequently the hNP breaks up. We obtain a maximum H/Pd ratio of 1.21 when H is introduced only inside the cavity. However, when H is deposited both on the inside and outside surfaces, this ratio reaches 1.70, which is 25% larger than previous reports. Beyond this ratio, the hNP breaks up, and the H gas is ejected from the hNP cavity.

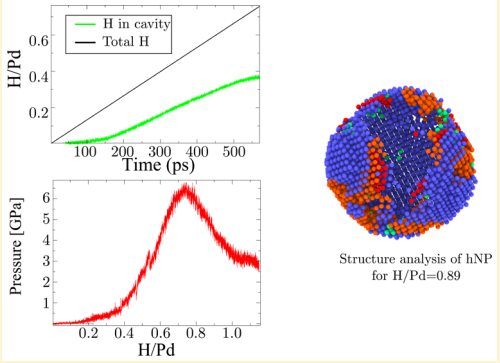

INTRODUCTION

Palladium-based structures have attracted much interest for a long time because of their major role in several industrial processes like catalysis, hydrogen storage, and gas-sensing. Moreover, during the last years, fuel cells based on Pd have been developed,[1] which have potential for many power supply applications in daily use devices, such as vehicles and cellphones. In these areas, Pd materials are an economically and competitive choice, especially when compared with other noble metals such as Pt.

In particular, the development of Pd nanostructures with large H storage capacity has been investigated for a variety of configurations such as nanowires,[2] nanorods, nanocubes,[3] and nanoparticles,[4−6] offering better performance than bulk structures,[7] thin films,[8] and grain boundaries.[9] Among all these morphologies nanoparticle (NP) show promising advantages for H storage, due their large surface to volume ratio, which allows for increased H capture. This led to many theoretical and experimental studies on the NP palladium H storage mechanism, and their variations with shape and size.[5,10−13]

Lately hollow nanoparticles (hNPs), which have a significantly lower density and a large specific area in comparison to conventional NPs, have attracted special attention due their potential applications in fields like catalysis, storage, sensors,[14] drug delivery,[15,16] and energy related devices. Moreover, recent experimental work has confirmed the potential of hNPs as storage material. In fact, hNPs of different materials such as Fe_2O_3,[17,18] SnO_2,[19] Si,[20] and TiO_2[21] have shown promissory results for Li storage,[17,18] which are essential for the development of efficient lithium batteries. Additionally, the H storage of Li_2NH hNP has been explored and shows an enhanced kinetics,[22] probably due to features like short diffusion distance and/or large surface area. These nanostructures can absorb a large amount of H in a shorter time than micrometer size particles. Moreover, the hydrogen desorption temperature can decrease by ≈100 K when compared to the bulk. Other examples are carbon and mesophorous carbon hNP decorated with Pd NPs,[23,24] which exhibit a larger storage capacity than pristine samples, reaching an increase of a factor of 2 of H weight. This has led us to investigate the feasibility of the use Pd hNP as a H storage material because of its H dissociation capacity under ambient conditions.

Currently, these Pd hNPs are synthesized by many groups, in a wide range of sizes.[14,25] For example, Liu et al.[26] reported raspberry-like hNPs of 32 nm diameter implanted in carbon nanotubes. Other groups reported hNPs with porous shells ≈25 nm in diameter created by the galvanic replacement method,[27] or ≈19 nm by the coalescence of smaller NPs.[28] Moreover, in the past few years, smaller quasi-spherical hNP have been fabricated by the reduction technique,[29] with an average diameter of 7.3 nm, but their thickness was not

Received: August 4, 2016
Revised: September 20, 2016
Published: September 26, 2016

DOI: 10.1021/acs.jpcc.6b07895
J. Phys. Chem. C 2016, 120, 23836−23841

reported. All these sizes are within the scope of classical molecular dynamics (MD) simulations, which can provide an accurate description of their mechanical and thermal properties.

Our main objective is the study of the H storage capacity of these hNPs. To achieve our goal, we deposit, one by one, H atoms in the hNP cavity until saturation is reached. To start on a firm basis, we obtain, by means of MD simulations, the thermal and mechanical properties of hNPs at 300 K. Since defects are generated during the hydrogenation process, we also investigate how they form.

METHODS

In order to understand the thermal and structural properties of Pd hNPs, we use classical MD simulations, as implemented in the LAMMPS code.[30] The simulations were carried out using the embedded atom[31] (EAM) potential, with the Zhou[32] parametrization. The hNP was created by cutting a spherical cavity from a face-centered cubic (fcc) Pd ⟨100⟩ bulk. This quasi-spherical geometry is characterized by the external radius R_{ext} and the shell thickness w. The range of radii studied is $6a_0 \leq R \leq 60a_0$ ($2.4 \leq R \leq 24$ nm), and thicknesses between $a_0 \leq w \leq 6a_0$ ($0.4 \leq R \leq 2.4$ nm), where $a_0 = 3.89$ Å is the Pd lattice parameter. Initially, alternating the Fast Inertial Relaxation Engine[33] (FIRE) and the Conjugate Gradient algorithms achieved the best possible putative minimum energy conformation. To study the thermal stability of these nanostructures, the temperature of the system was varied from 0 to 300 K, with an increase of 20 K every 0.2 ns. The system temperature was controlled by a Nose-Hoover thermostat, and a time-step of 1 fs was adopted.

To estimate the H storage capacity of these structures, atomic H was inserted into the hNP hole. In some experimental situations, H would be incorporated to the hNP from the outside. This would be extremely costly computationally. As an alternative, we have chosen to model the incorporation of H from the inside of the hNP, which allows faster H incorporation. Therefore, to estimate the H storage capacity of these structures, atomic H was inserted directly into the hNP hole. However, the EAM potential does not provide realistic results because the H−H interaction allows for the formation of H nanoclusters in the gas phase. A more realistic treatment for H in the gas phase is given by the ReaxFF potential[34] with the Senftle parametrization.[35] This potential has been fitted to reproduce hydrogen dissociation and migration in Pd, and has shown to be in good agreement with experiments[36,37] of H absorption from the gas phase, and the Pd NPs diffusion coefficients. The reactive nature of ReaxFF allows one to correctly reproduce the H−H interaction, without yielding the formation of H agglomerates. H was deposited at random at a distance of 0.5 a_0 from the inner hNP surface. Due to the mass difference between H and Pd, an adaptive time-step between 0.1 and 0.25 fs was chosen. The H pressure is computed evaluating the stress tensor, given by the relation

$$p_i^{\alpha\beta} = -\frac{1}{3}\mathrm{Tr}\left[\frac{m_i v_i^{\alpha} v_j^{\beta} + \sum_{i\neq j} F_{ij}^{\alpha} r_{ij}^{\beta}}{\Omega_i}\right] \quad (1)$$

where the first term is the thermal contribution, v_i^{α} is the α component of the ith atom velocity, Ω_i is the atomic volume, and F_{ij} and r_{ij} are the force and distance between atom i and j, respectively. The atomic volume Ω_i is estimated on the basis of the Pauling radius[38] assuming spherical atomic shape. This assumption yields similar results to other algorithms used to evaluate the atomic volume, as Voronoi tessellation.[39] Defects and/or fractures resulting from the H absorption, and the consequent pressure increase it generates, has been studied using the common neighbor analysis (CNA) algorithm,[40] which is the one implemented in the Open Visualization Tool[41] (OVITO). In addition, a more refined description of the crystal structure was obtained with the Crystal Analysis Tool[42] (CAT), which is a set of algorithms that advantageously use several postprocessing defect recognition methods, to generate a unique signature for each microstructure. These signatures are then matched against a pattern database, which not only contains information, but also allows one to determine the atomic positions relative to other crystalline structures, by means of graph maps.

RESULTS

Since our first objective is to describe the thermal stability of hNP, we start with perfect spherical hNPs of different sizes and thicknesses. As suggested by Jiang et al.,[43] when the hNP temperature is raised from 0 to 300 K the initial configuration can reach three possibles final outcomes: (i) a stable hNP, when it keeps its shape at the end of the temperature ramp; (ii) an unstable configuration, if it collapses to form a deformed solid NP at temperatures above 300 K; and finally (iii) a half-stable hNP, which is defined as a partial collapse of the initial configuration that maintains a cavity in its interior. The results for the different ratios and thicknesses w we studied are illustrated in Figure 1, where we provide a stability diagram for

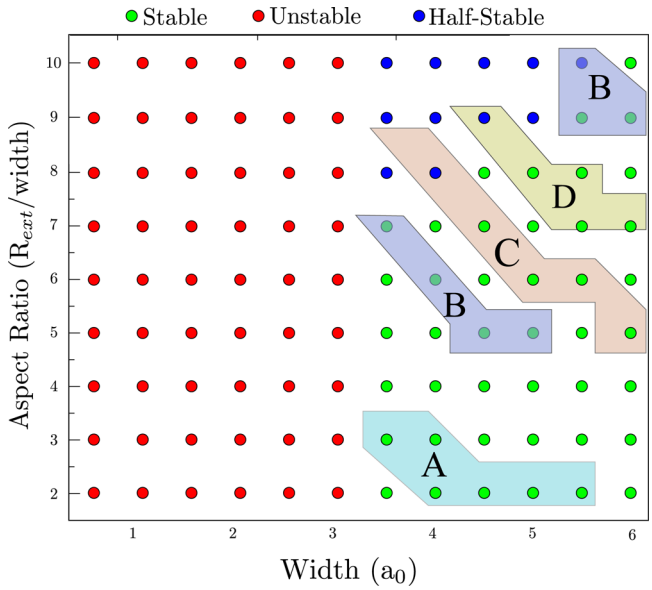

Figure 1. Stability diagram for Palladium nanoclusters using the EAM potential. The B region is in agreement with experimental results by Chen et al.[29] A corresponds to the experimental results reported by Wang et al.,[27] and C and D correspond to the results of Liu et al.[26] and Ge et al.,[28] respectively.

different sizes and thicknesses that are in agreement with experimental results.[28,29] The figure shows an unstable region for $w \leq 3a_0$ (red circles), a stable region (green circles), and half-stable hNPs (blue circles) are found only for large values of the aspect ratio, which is defined as R_{ext}/w. We also show an A zone where our theoretical values are consistent with the

DOI: 10.1021/acs.jpcc.6b07895
J. Phys. Chem. C 2016, 120, 23836−23841

experimental results by Wang et al. for 25 nm NPs. For small hNPs, the experiments by Chen et al.[29] reported 7 nm diameter hNPs; however, they did not provide the values of w. Our MD simulations yield that these hNPs have a minimal $w \approx 1.5$ nm. The D regions correspond to the experimental results by Ge et al.,[28] who used the same synthesis protocol to obtain two different sized Pd hNP of ≈40 nm and ≈15 nm in diameter, by changing the *ph* of the concentration. For 40 nm diameter, they report a thickness of 8 nm. Instead, in our calculations, we obtain 40 nm hNP with a minimal thickness of ≈2.1 nm. This suggests that it might be possible to synthesize thinner hNPs.

All in all, the structures mentioned above, and illustrated in Figure 1, were followed during long computer runs to ensure that they preserve their atomic structure, and are stable over large time periods. These calculations followed the scheme developed by Jiang et al.[43] but with a significantly more extended in time temperature ramp. In all cases, we made sure that the atomic structure, potential energy, and the mean square displacement remained constant.

To study the H absorption, we chose a 7528 Pd atom hNP with inner and outer radii $R_{in} = 4\ a_0$ and $R_{out} = 8\ a_0$, respectively. This hNP is well within the stability range of the diagram of Figure 1, so as to exclude a possible collapse due to the embrittlement caused by the H absorption. Since the H−H interaction at high densities is not realistically described by EAM, a reactive potential such as ReaxFF is a more adequate tool to model the system. However, the significant computational time required by ReaxFF makes it costly to model large hNPs. Therefore the stability results for Pd hNPs were obtained with the Zhou potential,[32] which has been used as a reference for ReaxFF calculations. After raising the temperature of the initial structure from 0 to 300 K, during 0.2 ns, the results yield stable hNPs, both for ReaxFF and EAM, for a hNP of $R_{in} = 4\ a_0$ and $R_{out} = 8\ a_0$.

Figure 2 illustrates the initial H deposition stages into the hNP cavity, showing that the saturation of subsurface

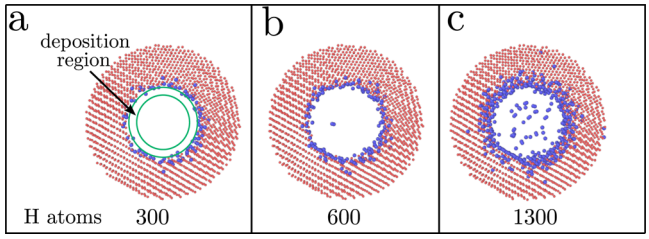

Figure 2. Cross section of Pd hNP (red atoms) used for the MD simulation of H (blue atoms) deposition. After 600 single atom depositions, the H atoms are repelled from the inner surface toward the center of the cavity. After 1300 H atoms are deposited, H_2 molecules and H atoms are observed in the center of the cavity.

octahedral and tetrahedral sites takes place first, followed by the saturation of the inner surface region. When the H atom absorption increases, a Pd hydride is seen to form on the inner surface, thereby reducing the inner cavity radius by almost 2 Å due to the Pd NP expansion; however, the hNP does not collapse. As a consequence of the formation of Pd hydride, the H absorption rate diminishes, and some of the atoms deposited are repelled from the inner shell toward the hNP cavity center, as seen in Figure 2b. The fact that the absorption time is reduced relative to the deposition time, due to hydride formation, promotes the formation of H_2 molecules, which creates a H gas phase in the cavity, as shown in Figure 2c.

In Figure 3a, we compare the H deposition with the H gas storage rates inside the cavity, as a function of time. For small

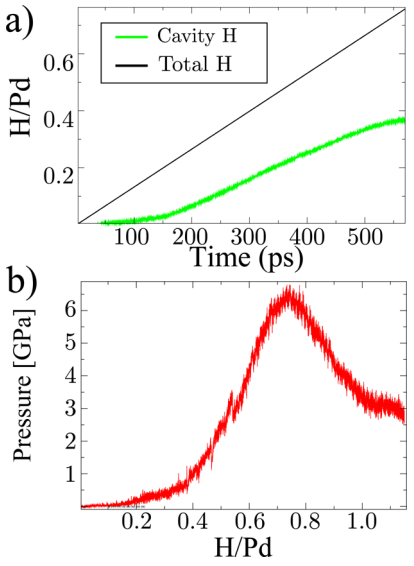

Figure 3. (a) Deposition rate as a function of time. The green curve corresponds to the H storage inside the cavity of the hNP. (b) Pressure in the cavity as a function of the H/Pd ratio.

values of the H/Pd ratio, all the H is absorbed in Pd interstitial sites; when H/Pd ≈ 0.2, an abrupt increase of H in the NP cavity is observed, which coincides with the formation of the Pd hydride. For large values of H/Pd, both the total and the cavity H have similar growth rates, thus the number of H_2 molecules and the H gas pressure do increase. The hydride helps to avoid the dissociation of H_2 molecules catalyzed by the Pd atoms. For H/Pd > 0.2, the mechanism for H insertion changes due to kinetic effects, as a consequence of the collisions of high speed H_2 molecules with H atoms. The collision of H_2 molecules with H atoms accelerates the latter enough to cross the inner hydride surface and to reach the outer layer of the hNP. Such a process was already reported for large values of the chemical potential, obtained by Monte Carlo simulations.[8,11−13]

The increment of the H density in the cavity results in a increase of the H pressure, which is not negligible for H/Pd > 0.2. The response of the structure to the pressure increase is a slow expansion of the hNP, whose radius grows by ≈2 Å. In Figure 3b we show that the maximum internal pressure that a hNP can withstand is 7 GPa; for larger H/Pd ratios, the pressure in the cavity decreases drastically to ≈3 GPa. This abrupt decrease is a consequence of structural changes in the hNP, such as creation of defects, amorphous regions, and stacking faults, which will be discussed below.

The response to pressure of the hNP as a function of the H/Pd ratio is illustrated in Figure 4. A common neighbor analysis (CNA) was performed before and after the pressure reached the 7 GPa peak. The pressure inside the cavity starts to create point defects in the Pd structure for H/Pd < 0.75, as shown in Figure 4a. These defects correspond to isolated bcc atoms near to the inner hNP radius; the red color atoms correspond to noncrystalline structures that are not well-defined, since for surface atoms they are not recognized as such by the CNA algorithm, as they lack the necessary coordination to be

DOI: 10.1021/acs.jpcc.6b07895
J. Phys. Chem. C 2016, 120, 23836−23841

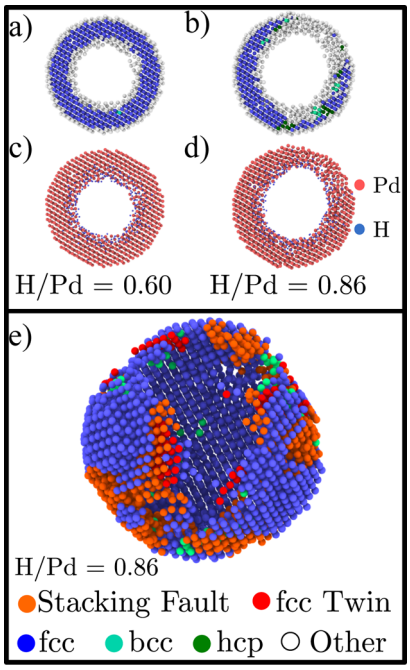

Figure 4. (a–d) Cross section of the hNP: (a,b) Common Neighbor Analysis (CNA) for two different Pd/H ratios; (c,d) H distribution inside the Pd lattice. (e) CAT analysis of the hNP with a H/Pd = 0.89; atoms with a structure type different from fcc or bcc were deleted from the picture.

identified as fcc. On the inner radius, the red region is wider than the surface one, due to the formation of Pd hydride. For H/Pd = 0.75, the hNP has also lost its spherical form, as shown in Figure 4c. A non-uniform width results, with a thinner region that has no definite crystalline structure. This region corresponds mainly to Pd hydride with some free volume regions, as shown in Figure 4d. It is worth noting that the porosity allows for a larger H storage capacity of the hNP. Moreover, for these concentrations, we observe a different scenario, where groups of hexagonal close packed (hcp) regions are seen in the Pd lattice. This hcp phase, whose occurrence in fcc crystals is principally associated with stacking faults, has been reported by Huang et al.[44] in AgPt hNPs, and is associated with Shockley partial dislocations, due to the large stress the hollow-core–shell structure is subjected to. In our case, the large stress produced by the H pressure can generate a series of planar defects, which under normal conditions are difficult to induce due the large energy required by Pd to generate stacking faults. This large population of hcp atoms are observed in the transition from stable to half-stable hNPs in Pd, and they are probably responsible for avoiding the collapse of the hNP into a simple NP. Figure 4e shows a CAT analysis where pattern-matching was performed including defective structures from a large database.[42] The fraction of fcc atoms obtained this way corresponds to 66.76%, and to 5.42% of fcc stacking fault and twin boundaries.

The feasibility to decorate the cavity of a Pd hNP has been tested by a single deposition process, resulting in a maximum H/Pd of 1.21. Beyond this limit, the hNP breaks up, and the H inside cavity is ejected. However, the hNP does not collapse, and a partial surface recovery is observed. The simulation was carried out during 0.2 ns, in order to be able follow the structural evolution of the hNP and the recovery of the surface. The fact that the hNP does not collapse after the H is released is a promising feature when one considers the possibility of reusing this kind of nanostructure. On the other hand, if the hNP cavity is preserved after the H ejection, both the inner and outer surface would be able to capture H, enhancing the hNP H storage capacity under ambient conditions.

Finally, to estimate the maximum H/Pd storage performance of Pd hNPs, we slightly changed the procedure. We started with an hNP with a H/Pd ratio of 1.1, which insures no material failure. This hNP was immersed in a H atmosphere, in order to accelerate the calculations. The H atoms occupy the free sites on the outer surface of the hNP allowing the H/Pd ratio to rise to 1.70, as illustrated in Figure 5. To ensure stability, the

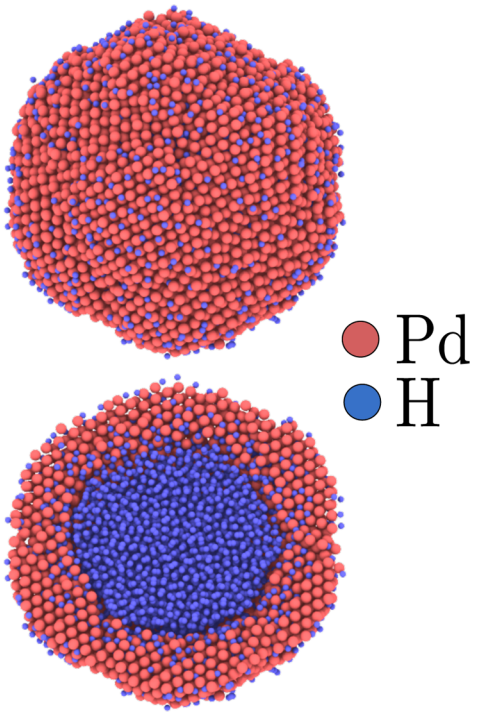

Figure 5. hNP after the H/Pd = 1.7 concentration is reached. Blue and red correspond to H and Pd, respectively. The top pannel corresponds to the outer surface, and the lower one to an equatorial cut.

dynamics was followed for ≈0.2 ns. To the best of our knowledge, this is the largest value reported for a Pd nanostructure, since the previous one, obtained by means of Monte Carlo simulations,[8,11−13] is 1.33.

DISCUSSION AND CONCLUSIONS

By means of molecular dynamics simulations, we investigate the stability of Pd hNP, from 0.3 to 2.3 nm in thickness and less than 42 nm in diameter. Our stability diagram shows that it is possible to observe a transition of the hNP from unstable to stable when a thickness of $w \approx 1.17$ nm is reached (which corresponds to 3 a_0 in Figure 1). For $w > 1.17$ nm, the hNP stability increases. For $w < 1.17$ nm, the hNP tends to collapse and form a solid NP. This result is similar to the one reported by Jiang et al.[45] for Au hNP. In fact, our simulations predict stable hNP with diameters larger than 5.5 nm and a minimum thickness of 1.4 nm, smaller than those reported by Chen et al.[29] The largest hNPs we studied were 42 nm in diameter and $w > 2.3$ nm, establishing a lower limit for the Pd hNP synthesized by Ge et al.[28] of 40 nm with a thickness of 8 nm.

DOI: 10.1021/acs.jpcc.6b07895
J. Phys. Chem. C 2016, 120, 23836−23841

Other experimental results, as those reported by Liu et al.[26] and Wang et al.,[27] also correspond to stable Pd hNP in our diagram.

On the other hand, the H storage properties of hNP have been tested, introducing single H atoms into the hNP cavity. Our results show that the cavity can store H in the form of single atoms or as a H gas phase. This gas phase is achieved when Pd hydride is formed on the inner surface and the deposition rate is larger than the H absorption rate. The hNP studied here can withstand a H pressure of up to 7 GPa. Beyond this limit, the hNP changes its shape in order to relax the large stress the H_2 gas pressure generates. The defects observed correspond mainly to stacking faults and twins. The latter ones have been reported to induce ultrahigh hardening of Pd thin films.[46] This way, the maximum H/Pd ratio of 1.21 is reached. Beyond this limit, the hNP breaks up, and H_2 it is ejected from the cavity. As the H is released, the hNP partially recovers without collapsing.

Finally, a maximum H/Pd = 1.7 ratio is obtained when single H atoms are deposited on the outer and inner surfaces of the hNP. This ratio is the largest yet reported, and is 25% larger than the results for an icosahedron cluster obtained by Crespo et al.[11] However, we believe that this results could be improved, for example, using MC simulations to decorate the Pd interstitial sites.[8,11−13]

Summarizing, we studied the efficiency of Pd hNPs to store H inside their cavities and in the whole structure. However, important questions that deserve attention remain open, such as the details of the diffusion mechanism in this kind of nanostructures. It also may be that the presence of stacking faults and/or twins helps to increase the H migration and absorption. But, for the time being, our results suggest that the use of the cavity of a hNP as a gas storage material is a possibility, and a subject that deserves attention.

AUTHOR INFORMATION

Corresponding Author

*Phone: +562 2978 7290; E-mail: m.kiwi.t@gmail.com.

Notes

The authors declare no competing financial interest.

ACKNOWLEDGMENTS

This work was supported by the Fondo Nacional de Investigaciones Científicas y Tecnológicas (FONDECYT, Chile) under grants #3140526 (RG), #1160639 and 1130272 (MK and JR), and Financiamiento Basal para Centros Científicos y Tecnológicos de Excelencia FB-0807 (RG, FV, JM, MK and JR). EMB and DT thank support from PICT-2014-0696 (ANPCyT) and M003 (SeCTyP-UN Cuyo) grant. DT was supported by CONICET Postdoctoral Fellowship Grant and ANPCyt PICT-2015-0040. FV was supported by CONICYT Doctoral Fellowship grant #21140948.

REFERENCES

(1) Antolini, E. Palladium in Fuel Cell Catalysis. *Energy Environ. Sci.* **2009**, *2*, 915−931.

(2) He, J.; Knies, D.; Hubler, G.; Grabowski, K.; Tonucci, R.; Dechiaro, L. Hydrogen Segregation and Lattice Reorientation in Palladium Hydride Nanowires. *Appl. Phys. Lett.* **2012**, *101*, 153103.

(3) Nie, G.; Lu, X.; Lei, J.; Yang, L.; Bian, X.; Tong, Y.; Wang, C. Sacrificial Template-Assisted Fabrication of Palladium Hollow Nanocubes and Their Application in Electrochemical Detection toward Hydrogen Peroxide. *Electrochim. Acta* **2013**, *99*, 145−151.

(4) Narehood, D.; Kishore, S.; Goto, H.; Adair, J.; Nelson, J.; Gutierrez, H.; Eklund, P. X-ray Diffraction and H-storage in Ultra-Small Palladium Particles. *Int. J. Hydrogen Energy* **2009**, *34*, 952−960.

(5) Wolf, R. J.; Lee, M. W.; Ray, J. R. Pressure-Composition Isotherms for Nanocrystalline Palladium Hydride. *Phys. Rev. Lett.* **1994**, *73*, 557.

(6) Yamauchi, M.; Ikeda, R.; Kitagawa, H.; Takata, M. Nanosize Effects on Hydrogen Storage in Palladium. *J. Phys. Chem. C* **2008**, *112*, 3294−3299.

(7) Conrad, H.; Ertl, G.; Latta, E. Adsorption of Hydrogen on Palladium Single Crystal Surfaces. *Surf. Sci.* **1974**, *41*, 435−446.

(8) Ramos De Debiaggi, S.; Crespo, E.; Braschi, F.; Bringa, E.; Alí, M.; Ruda, M. Hydrogen Absorption in Pd Thin-Films. *Int. J. Hydrogen Energy* **2014**, *39*, 8590−8595.

(9) Kuji, T.; Matsumura, Y.; Uchida, H.; Aizawa, T. Hydrogen Absorption of Nanocrystalline Palladium. *J. Alloys Compd.* **2002**, *330*, 718−722.

(10) Pundt, A.; Dornheim, M.; Guerdane, M.; Teichler, H.; Ehrenberg, H.; Reetz, M.; Jisrawi, N. Evidence for a Cubic-to-Icosahedral Transition of Quasi-Free Pd-H-Clusters Controlled by the Hydrogen Content. *Eur. Phys. J. D* **2002**, *19*, 333−337.

(11) Crespo, E. A.; Ruda, M.; Ramos de Debiaggi, S.; Bringa, E. M.; Braschi, F. U.; Bertolino, G. Hydrogen Absorption in Pd Nanoparticles of Different Shapes. *Int. J. Hydrogen Energy* **2012**, *37*, 14831−14837.

(12) Crespo, E.; Claramonte, S.; Ruda, M.; de Debiaggi, S. R. Thermodynamics of Hydrogen in Pd Nanoparticles. *Int. J. Hydrogen Energy* **2010**, *35*, 6037−6041.

(13) Ruda, M.; Crespo, E.; Ramos de Debiaggi, S. Atomistic Modeling of H Absorption in Pd Nanoparticles. *J. Alloys Compd.* **2010**, *495*, 471−475.

(14) Liang, H.-P.; Lawrence, N. S.; Wan, L.-J.; Jiang, L.; Song, W.-G.; Jones, T. G. Controllable Synthesis of Hollow Hierarchical Palladium Nanostructures with Enhanced Activity for Proton/Hydrogen Sensing. *J. Phys. Chem. C* **2008**, *112*, 338−344.

(15) Son, S. J.; Bai, X.; Lee, S. B. Inorganic Hollow Nanoparticles and Nanotubes in Nanomedicine: Part 1. Drug/gene Delivery Applications. *Drug Discovery Today* **2007**, *12*, 650−656.

(16) Son, S. J.; Bai, X.; Lee, S. B. Inorganic Hollow Nanoparticles and Nanotubes in Nanomedicine: Part 2: Imaging, Diagnostic, and Therapeutic Applications. *Drug Discovery Today* **2007**, *12*, 657−663.

(17) Koo, B.; Xiong, H.; Slater, M. D.; Prakapenka, V. B.; Balasubramanian, M.; Podsiadlo, P.; Johnson, C. S.; Rajh, T.; Shevchenko, E. V. Hollow Iron Oxide Nanoparticles for Application in Lithium Ion Batteries. *Nano Lett.* **2012**, *12*, 2429−2435.

(18) Wang, B.; Chen, J. S.; Wu, H. B.; Wang, Z.; Lou, X. W. Quasiemulsion-Templated Formation of α-Fe2O3 Hollow Spheres with Enhanced Lithium Storage Properties. *J. Am. Chem. Soc.* **2011**, *133*, 17146−17148.

(19) Lou, X. W.; Wang, Y.; Yuan, C.; Lee, J. Y.; Archer, L. A. Template-free Synthesis of SnO2 Hollow Nanostructures with High Lithium Storage Capacity. *Adv. Mater.* **2006**, *18*, 2325−2329.

(20) Ma, H.; Cheng, F.; Chen, J.-Y.; Zhao, J.-Z.; Li, C.-S.; Tao, Z.-L.; Liang, J. Nest-like Silicon Nanospheres for High-Capacity Lithium Storage. *Adv. Mater.* **2007**, *19*, 4067−4070.

(21) Chen, J. S.; Luan, D.; Li, C. M.; Boey, F. Y. C.; Qiao, S.; Lou, X. W. TiO 2 and SnO 2@ TiO 2 Hollow Spheres Assembled from Anatase TiO 2 Nanosheets with Enhanced Lithium Storage Properties. *Chem. Commun.* **2009**, *46*, 8252−8254.

(22) Xie, L.; Zheng, J.; Liu, Y.; Li, Y.; Li, X. Synthesis of Li2NH Hollow Nanospheres with Superior Hydrogen Storage Kinetics by Plasma Metal Reaction. *Chem. Mater.* **2008**, *20*, 282−286.

(23) Zielinska, B.; Michalkiewicz, B.; Mijowska, E.; Kalenczuk, R. J. Advances in Pd Nanoparticle Size Decoration of Mesoporous Carbon Spheres for Energy Application. *Nanoscale Res. Lett.* **2015**, *10*, 430.

(24) Wenelska, K.; Michalkiewicz, B.; Gong, J.; Tang, T.; Kaleńczuk, R.; Chen, X.; Mijowska, E. In situ Deposition of Pd Nanoparticles with Controllable Diameters in Hollow Carbon Spheres for Hydrogen Storage. *Int. J. Hydrogen Energy* **2013**, *38*, 16179−16184.

DOI: 10.1021/acs.jpcc.6b07895
J. Phys. Chem. C 2016, 120, 23836−23841

(25) Kim, S.-W.; Kim, M.; Lee, W. Y.; Hyeon, T. Fabrication of Hollow Palladium Spheres and their Successful Application to the Recyclable Heterogeneous Catalyst for Suzuki Coupling Reactions. *J. Am. Chem. Soc.* **2002**, *124*, 7642−7643.
(26) Liu, Z.; Zhao, B.; Guo, C.; Sun, Y.; Shi, Y.; Yang, H.; Li, Z. Carbon Nanotube/Raspberry Hollow Pd Nanosphere Hybrids for Methanol, Ethanol, and Formic Acid Electro-Oxidation in Alkaline Media. *J. Colloid Interface Sci.* **2010**, *351*, 233−238.
(27) Wang, B.; Yang, J.; Wang, L.; Wang, R.; Tian, C.; Jiang, B.; Tian, M.; Fu, H. Hollow Palladium Nanospheres with Porous Shells Supported on Graphene as Enhanced Electrocatalysts for Formic Acid Oxidation. *Phys. Chem. Chem. Phys.* **2013**, *15*, 19353−19359.
(28) Ge, J.; Xing, W.; Xue, X.; Liu, C.; Lu, T.; Liao, J. Controllable Synthesis of Pd Nanocatalysts for Direct Formic Acid Fuel Cell (DFAFC) Application: from Pd Hollow Nanospheres to Pd Nanoparticles. *J. Phys. Chem. C* **2007**, *111*, 17305−17310.
(29) Chen, D.; Cui, P.; He, H.; Liu, H.; Yang, J. Highly Catalytic Hollow Palladium Nanoparticles Derived from Silver@Silver-Palladium Core-Shell Nanostructures for the Oxidation of Formic Acid. *J. Power Sources* **2014**, *272*, 152−159.
(30) Plimpton, S. Fast Parallel Algorithms for Short-Range Molecular Dynamics. *J. Comput. Phys.* **1995**, *117*, 1−19.
(31) Daw, M. S.; Baskes, M. I. Embedded-Atom Method: Derivation and Application to Impurities, Surfaces, and other Defects in Metals. *Phys. Rev. B: Condens. Matter Mater. Phys.* **1984**, *29*, 6443.
(32) Zhou, X.; Zimmerman, J. A.; Wong, B. M.; Hoyt, J. J. An Embedded-Atom Method Interatomic Potential for Pd-H Alloys. *J. Mater. Res.* **2008**, *23*, 704−718.
(33) Bitzek, E.; Koskinen, P.; Gähler, F.; Moseler, M.; Gumbsch, P. Structural Relaxation Made Simple. *Phys. Rev. Lett.* **2006**, *97*, 170201.
(34) Van Duin, A. C.; Dasgupta, S.; Lorant, F.; Goddard, W. A. ReaxFF: a Reactive Force Field for Hydrocarbons. *J. Phys. Chem. A* **2001**, *105*, 9396−9409.
(35) Senftle, T. P.; Janik, M. J.; van Duin, A. C. A ReaxFF Investigation of Hydride Formation in Palladium Nanoclusters via Monte Carlo and Molecular Dynamics Simulations. *J. Phys. Chem. C* **2014**, *118*, 4967−4981.
(36) Langhammer, C.; Zhdanov, V. P.; Zorić, I.; Kasemo, B. Size-Dependent Kinetics of Hydriding and Dehydriding of Pd Nanoparticles. *Phys. Rev. Lett.* **2010**, *104*, 135502.
(37) Hara, S.; Caravella, A.; Ishitsuka, M.; Suda, H.; Mukaida, M.; Haraya, K.; Shimano, E.; Tsuji, T. Hydrogen Diffusion Coefficient and Mobility in Palladium as a Function of Equilibrium Pressure Evaluated by Permeation Measurement. *J. Membr. Sci.* **2012**, *421*, 355−360.
(38) Pauling, L. *The Nature of the Chemical Bond and the Structure of Molecules and Crystals: An Introduction to Modern Structural Chemistry*; Cornell University Press: Ithaca, NY, 1960; Vol. *18*.
(39) Du, Q.; Faber, V.; Gunzburger, M. Centroidal Voronoi Tessellations: Applications and Algorithms. *SIAM Rev.* **1999**, *41*, 637−676.
(40) Honeycutt, J. D.; Andersen, H. C. Molecular Dynamics Study of Melting and Freezing of Small Lennard-Jones Clusters. *J. Phys. Chem.* **1987**, *91*, 4950−4963.
(41) Stukowski, A. Visualization and Analysis of Atomistic Simulation Data with OVITO-the Open Visualization Tool. *Modell. Simul. Mater. Sci. Eng.* **2010**, *18*, 015012.
(42) Stukowski, A. Structure Identification Methods for Atomistic Simulations of Crystalline Materials. *Modell. Simul. Mater. Sci. Eng.* **2012**, *20*, 045021.
(43) Jiang, L.; Yin, X.; Zhao, J.; Liu, H.; Liu, Y.; Wang, F.; Zhu, J.; Boey, F.; Zhang, H. Theoretical Investigation on the Thermal Stability of Hollow Gold Nanoparticles. *J. Phys. Chem. C* **2009**, *113*, 20193−20197.
(44) Huang, R.; Shao, G.-F.; Zeng, X.-M.; Wen, Y.-H. Diverse Melting Modes and Structural Collapse of Hollow Bimetallic Core-Shell Nanoparticles: A Perspective from Molecular Dynamics Simulations. *Sci. Rep.* **2014**, *4*, 7051.
(45) Jiang, S.; Zhang, Y.; Gan, Y.; Chen, Z.; Peng, H. Molecular Dynamics Study of Neck Growth in Laser Sintering of Hollow Silver Nanoparticles with Different Heating Rates. *J. Phys. D: Appl. Phys.* **2013**, *46*, 335302.
(46) Idrissi, H.; Wang, B.; Colla, M. S.; Raskin, J. P.; Schryvers, D.; Pardoen, T. Ultrahigh Strain Hardening in Thin Palladium Films with Nanoscale Twins. *Adv. Mater.* **2011**, *23*, 2119−2122.

DOI: 10.1021/acs.jpcc.6b07895
J. Phys. Chem. C 2016, 120, 23836−23841